SURFACE ROUGHENING MECHANISMS FOR TUNGSTEN EXPOSED TO LASER, ION, AND X-RAY PULSES

Michael Andersen and Nasr M. Ghoniem

University of California Los Angeles (UCLA) 420 Westwood Plaza/48-121, Los Angeles, CA 90095-1597
M.Andersen@ucla.edu.

Tungsten is a candidate material for a variety of applications in Magnetic and Inertial Fusion Energy systems. Experimental data show that the surface of tungsten exposed to laser, ion, and X-ray irradiation undergoes substantial roughening. Control of surface conditions is essential to the design of these systems, since it can lead to crack formation, adverse effects on heat absorption because of emissivity changes, and eventual failure.

We first review recent experimental data on the effects of laser, ion and X-ray energetic pulses on the evolution of a surface to identify the variety of patterns and length scales and their dependence on the type and magnitude of irradiation pulses. Then we present a model for the evolution of surface roughness as a result of the balance between destabilizing elastic strain energy caused by thermomechanical strains and near surface accumulation of defects on the one hand, and stabilizing surface and near surface atomic diffusion on the other. Results of the model determine the conditions for surface roughness evolution and the effects of radiation fluence and pulse intensity on surface morphology.

I. INTRODUCTION

Roughening and grooving of solid surfaces has been researched to some extent in fields such as chemical etching[1] and heteroepitaxial thin film growth,[2] where an interface between phases is present. Both have an atomic-level description, which explains the surface conditions. In chemical etching the solid is in contact with its melt creating direct diffusion of atoms on the surface either into or out of the solid. In the case of heteroepitaxy, where thin films are grown on crystalline substrates, atoms move along the surface in the solid-vacuum region. The source of the axial stress comes from the lattice mismatch.[3] The movement is created by a gradient in the chemical potential and is seen in processes involving high stress, high temperature, and small-size scales.[4]

An initially flat surface is found to be unstable with respect to morphological perturbations on the surface. Under all these conditions, it has been recognized that the driving force for the instability is the reduction in the elastic energy of the solid when its surface becomes corrugated. Thus, flat surfaces tend to develop cusps and valleys when a threshold level of stress is applied. A model can be developed from this characteristic based on the original Asaro-Tiller-Grinfeld (ATG) instability theory.[5] These models are based on coupling the diffusion field of subsurface vacancies generated in the material with the strain field derived from the elasticity theory. Because generated vacancies have a drift component superimposed on their random lateral motion in the subsurface layer, they tend to aggregate non-uniformly underneath the surface, creating surface corrugations (roughening transitions) that can be directly verified experimentally at LLNL and at Sandia Labs on X-ray and ion effects. It is therefore important to develop a model that would help predict when a radiated surface will begin to fail.

Previous work has been undertaken to predict failures from crack growth, but little has been researched to determine when the crack will nucleate. The latter is significant, since once the crack forms, the material is very near failure. Measuring the surface roughness and gaining an understanding of how the surface progresses under the thermal loading would provide a way to help determine the life-before-crack. If we focus on the ATG instability, we must first determine a method for finding the strain energy and thus associated stresses from the loading. For these stresses, a boundary element method (BEM) will be utilized to save computing time. The focus of this paper is two-fold. First, the model description will be explained including the self-diffusion mechanism and stress calculations. Second, the ground work will be set for further advancements in 2D and a path to 3D will be detailed.

I.A. Experimental Influence

There are three test facilities providing experimental data for the HAPL program. The University of California San Diego (UCSD) has a 0.5 kJ laser operating at 10 Hz

called Dragonfire. Lawrence Livermore National Lab (LLNL) is able to check X-ray influence using its XAPPER and finally Sandia National Labs (SNL) uses its RHEPP program to examine ion exposure. All programs use the same single crystal or powder met tungsten samples provided by Oak Ridge National Laboratory and are able to map surface roughness along with temperature.

I.A.1. Repetitive High Energy Pulsed Power (RHEPP)

In future laser driven IFE power plants it is expected that the first wall armor will experience ions with fluences on the order of 20 J/cm^2. The effects of these MeV-level ions are simulated at SNL on various forms of tungsten dry-wall materials using the RHEPP-1. Details on the beam can be found from papers published by T. Renk.[6] Measurements of surface roughening are found by using 1 and 2-dimensional profilometry (Fig. 1).

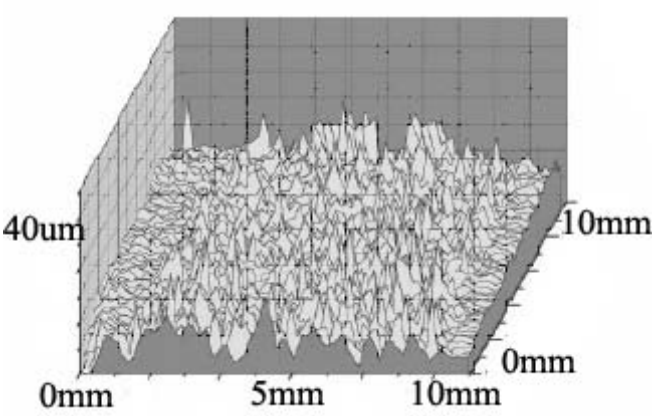

Fig. 1. Scan of PM-W surface using a NEXIV Laser Interferometer, 1600 pulses at an average of 1.5 J/cm^2. The roughness defined from peak to valley can reach around 5-10 μm (Ref. 6).

The ions penetrate several microns into the samples causing rapid heating and rapid cooling (10^9 K/sec). At high fluences, the surface experiences sublimation and/or ablation and the composition change of roughly a monolayer of ions (~10^{14}/cm^2) at a depth of about 1 micron. The response of the samples differ quite dramatically as the roughening threshold for powder metallurgy (PM) W was measured at 1.25 J/cm^2 and above 3 J/cm^2 for W alloyed with 25% Re (W25Re) with as little as 75 pulses.[7] The surface roughness seems to change depending on the initial topology and in some cases actually decreases. When the fluence increases pass the thresholds, the roughness, Ra, increases quite rapidly. At 3.7 J/cm^2 the roughness reaches 20 μm with Peak-to-Valley (P-V) measurements exceeding 70 μm. It should be noted that the roughening threshold changes depending on the penetrating ion, but in general roughness increases with number of pulses and fluence. Even though samples were kept below the melting temperature, they still roughened suggesting the effect of thermomechanical stress.[8]

I.A.I1. X-ray Ablation with Plasma Pinch in the EUV Region (XAPPER)

LLNL is experimenting with the X-ray threshold for tungsten using their XAPPER facility. Using the same temperature profile as seen in IFE (fig. 2), LLNL is trying to replicate the same energy spike. Details on the exact specifications of the XAPPER can be found in papers by Latkowski et al.[9]

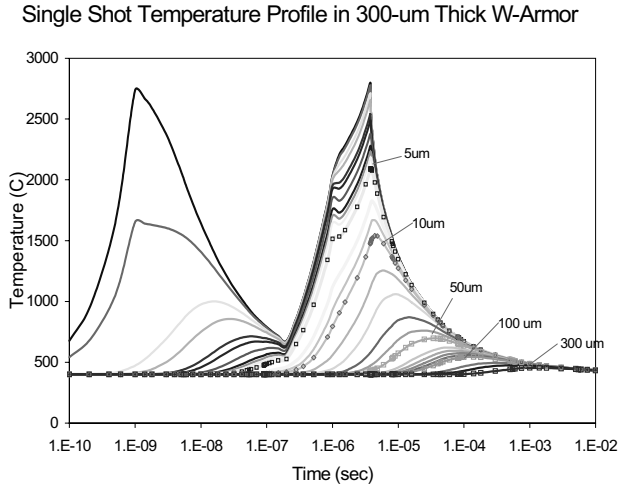

Fig. 2. Time dependent temperature of a tungsten coated ferritic steel chamber wall following micro-explosion of a DT-pellet in an IFE chamber. Each contour line is 1 micron into the material showing a total of 300 contours (W: 300 μm, Steel: 3 mm, chamber radius 6.5 m).

The fluence generated is on the order of 1.0 J/cm^2 with the spot size of about 1 mm. Roughening estimations are made using a Veeco white-light interferometer (WLI) showing initial roughness of the samples to be around 10-20 nm. Calculations from the XAPPER X-ray spectrum show that a fluence of 0.8 J/cm^2 is needed to model the necessary temperature profile. This fluence gives a peak temperature of 3250 K for an initial temperature of 773 K. During testing of the tungsten samples, the fluences ranged from 0.5 to about 1.2 J/cm^2, with pulse values from single-shot to as many as 10^5 in a given location. All samples are irradiated at room temperature, but with successive pulses the temperature rises about 300 degrees. After irradiation the samples appeared discolored, but for fluences around 0.7 J/cm^2 there is no statistical roughening. The single crystal may have even smoothed.[9] There was no measurable roughness until a fluence of 1.0 J/cm^2 was applied, which means that X-rays should have minimal roughening effect under expected IFE conditions. This is mainly due to the short-pulse nature of

the X-ray loading, which is on the order of nanoseconds. It may be worthwhile and ultimately necessary to analyze the effect of ion exposure on the tungsten after it has been irradiated with X-rays.

I.A.II1. Dragonfire at UCSD

The laser system at UCSD is important because it can mimic the effects of the X-rays and ions without creating a "harsh environment." A properly shaped laser pulse can match the same temperature profiles as witnessed in IFE conditions with the benefit of large numbers of pulses at high repetition rates.[10] UCSD also has an optical thermometer that can measure the real time temperature behavior of the exposed surface.

The Dragonfire system has recorded roughening in nearly all the test conditions for large number of pulses. The higher the change in temperature brings about roughening for fewer pulses. The peak temperature seems to have little effect compared to the change in temperature which supports that the roughening mechanism is the thermomechanical fatigue. Figure 3 shows that the roughening is associated with number of pulses, but more importantly, higher changes in temperatures create deeper grooving. It also appears that the grooves follow grain boundaries, and it should be noted that the spacing between the grooves appears relatively constant.

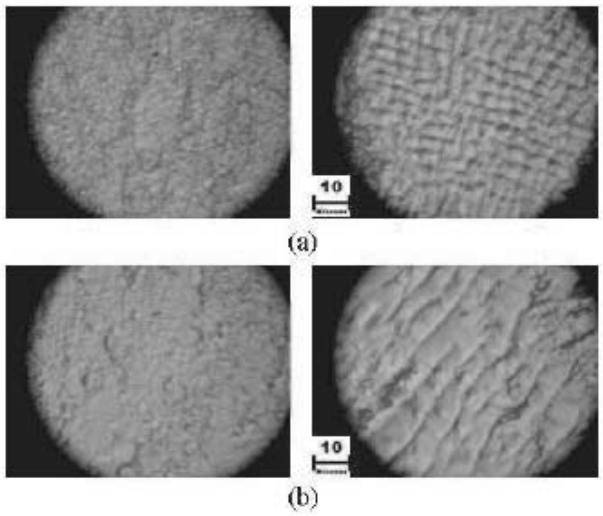

Fig. 3. The micrographs on the left show 1,000 pulses while the micrographs on the right show 10,000 pulses. (a) Temperature change of 1400 K during exposure, (b) temperature change of 1900 K. The higher temperature change in (b) leads to deeper roughening. Figures are taken from HAPL presentation given by F. Najmabadi in June 2005. It can be found at the following site: www-ferp.ucsd.edu/NAJMABADI/TALKS/HAPL/0506-HAPL-Exp.ppt.

These three test facilities provide concrete evidence for roughening that can be used as a benchmark for the roughening model. For instance, if 1600 pulses create an average roughness of 10-20 mm, then these conditions can be replicated in the model and the two can be compared.

I.B. Surface Kinetics

In order to study the evolution of the surface profile, a description of the chemical potential and how it applies to material transport needs to be established. The chemical potential, μ, can be described in a similar manner as Srolovitz[11] as

$$\mu = \mu^* + \gamma\Omega\kappa + \Omega\omega \tag{1}$$

where μ* is the chemical potential of a flat surface bounding the solid with bulk stress σ^o, γ is the surface energy, Ω is the atomic volume, κ is the surface curvature found from derivatives of the surface profile, and ω is the strain energy. The strain energy is found from Hooke's law as:

$$\begin{aligned} \omega &= \frac{1}{2}\varepsilon_{ij}\sigma_{ij} \\ \omega_b &= \frac{\left(1-\nu^2\right)}{E}\sigma^{\infty} \\ \omega_s &= \frac{1}{2E}\sigma_{tt}^2 \end{aligned} \tag{2}$$

where ω_b is the bulk strain energy and ω_s is the surface strain energy for plane strain. As it turns out, determining the stress on the surface becomes one of the more difficult tasks. A flat surface is relatively straight forward, but when the morphology begins to change, a modeling method is needed. In this case, a boundary element method will be used and explained in the next section. The surface material transport is determined by the Nernst-Einstein relation of the diffusion flux proportional to the surface gradient of the chemical potential given as

$$J = -\frac{D_s}{kT}\frac{\partial\mu}{\partial s} \tag{3}$$

where D_s is the surface diffusivity, k is the Boltzmann's constant, T is the absolute temperature and the derivative with respect to the arc length, s, is evaluated along the surface. The normal velocity of the surface V_n, is then proportional to the divergence of J:

$$V_n = -\frac{D_s\Omega\nu_s}{kT}\frac{\partial^2\mu}{\partial s^2} \tag{4}$$

where ν_s is the number of atoms per unit area of the material in the plane normal to the flux direction. This can be extended to the surface profile h(x,t) as

$$\frac{\partial h}{\partial t} = D\frac{\partial}{\partial x}\left[\left(1+h_x^2\right)^{-\frac{1}{2}}\frac{\partial}{\partial x}\left(\gamma\kappa+\omega\right)\right] \qquad (5)$$

where D is

$$D = \frac{D_s \nu_s \Omega^2}{kT} \qquad (6)$$

I.C. Boundary Element Method (BEM)

A key component of this problem is determining the stress along the surface as the morphology changes. This was first approximated with general elasticity, but needed to be more clearly defined around the changes in the surface. As the valleys deepen toward a crack, the stress increases dramatically so a method was needed to solve for these stresses. Boundary element method is used based upon discretizing only the surface instead of the whole volume. This makes it much easier to code and follow changing surfaces. The defining equation for this method is shown below

$$\int_S \overline{T}_{ij}\left(x,\xi\right)u_j\left(\xi\right)dS\left(x\right) \qquad (6)$$

where T is the elastic Green's function that satisfies the periodic boundary conditions and u is the displacement field. The key to this method is that it discretizes only over the surface reducing the calculation time and complexity. Stresses can be found inside the material nonetheless. More information can be found from Becker's book on the material.[11]

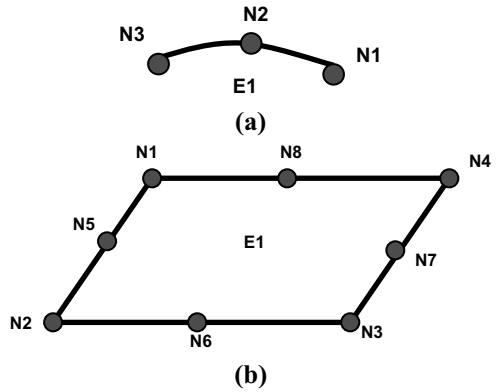

Fig. 4. Shown are two sample elements used in the BEM. (a) Shows a 2D element with 3 nodes listed in counter-clockwise direction. (b) Shows a 3D element with 8 nodes located at the corners and middle segments. Again, they are listed in counter-clockwise direction. The middle segment nodes are only needed for additional precision.

In the 2D case the connectivity of each element is 3, meaning that there is a node at each end point and one in the center of each element. Only x and y coordinates are needed as each element segment is on one plane. The nodal connectivity must be listed in counter clockwise direction such that the normal always points away from the surface. Double nodes can be added at the corners for greater precision. Stresses inside the boundary can be found, but they contain a 1/r parameter that leads to a singularity as the surface is approached. A more accurate way is used to find surface stresses by differentiating the surface displacements.

As far as the 3D BEM, the z coordinate is needed for the nodes and the connectivity for each element increases either to 4 nodes or 8 depending on the necessary precision. Figure (4) shows example elements from 2D and 3D showing the connectivity and placement of the nodes.

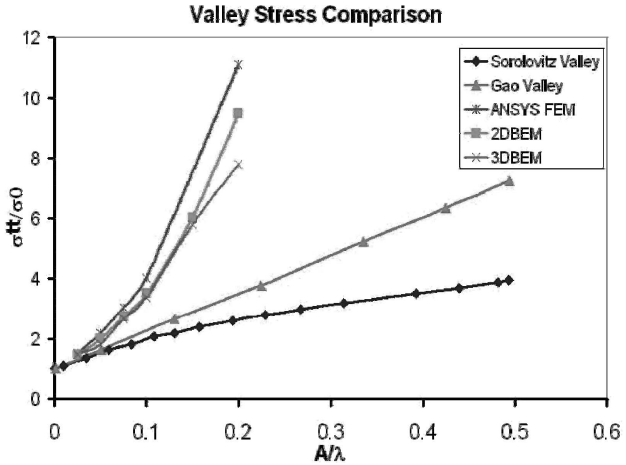

Fig. 5. Tangential stress at the valley of the roughened zone is shown to increase quite dramatically as ratio of the amplitude to wavelength increases. This is as expected as local stress around the valley would eventually approach that of a crack tip.[11,13]

As a validation to how well the BEM works, it is compared to a FEM analysis (ANSYS). The tested condition has applied axial stress corresponding to a temperature of 1500K with a seeded roughness from a cosine wave. Figure 5 shows the calculation of the stress at the valley compared to the applied stress. As can be seen, the 2D BEM, 3D BEM, and FEM all compare quite favorably. The initial surface has an amplitude to wavelength ratio of 0.05. Here the stresses found from each method are used in the surface kinetics and the surface is tracked. As can be seen in figure 6, they agree quite well showing that the BEM is just as good as FEM

for this work. The BEM has the advantage of being programmable with automatic surface changes without the recurring user interface needed with FEM.

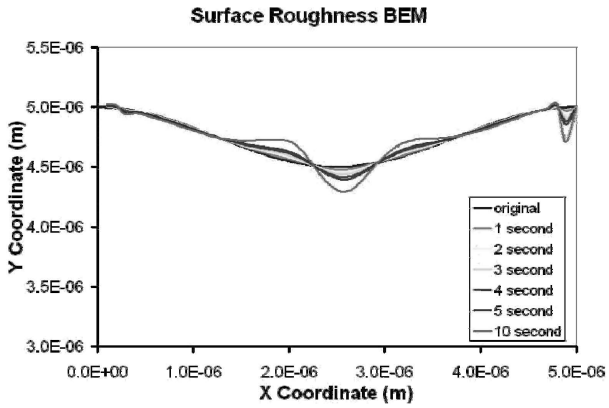

(a)

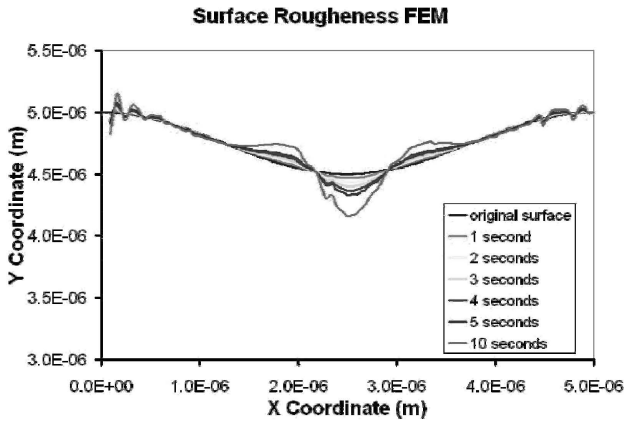

(b)

Fig. 6. (a) Shows the evolution of the surface using stresses calculated from the 2D BEM while (b) shows the surface with stresses found from FEM. An equal number of elements were used along the surface in each case. The calculation time for the stresses using BEM was a fraction of the time used for the FEM.

II. STATUS REPORT

The 2D BEM needs further refinements before it can be considered fully developed, including transient inclusion, long-time runs, effects of plasticity, and the possible addition of defects around the crack tip. Previous research has stopped once the roughness begins to form. The curvature and stress approach extreme values and calculations become too expensive to continue the growth. By including plasticity and consequent dislocations and blunting, we can control these stresses and continue the nucleation.

The work eventually needs to be extended to 3D where the derivatives over the surface become slightly more complicated as the Laplace-Beltrami operator must be used to find the derivatives of the chemical potential. The curves will have to be described using cubic splines. The key to this work will be the BEM because as the surface changes, the stress calculation will become more and more difficult. The calculations will be possible because the BEM only requires meshing and discretizing the surface.

ACKNOWLEDGMENTS

Funding to UCLA by the US Naval Research Laboratories (NRL) through the High Average Laser Program (HAPL) is greatly acknowledged (award number US NAVY N00173031G904).

REFERENCES

1. H.M. YANG and D.J. SROLOVITZ. *Phys Rev Letters*, **71**, (10):1593-1596 (1993).
2. KLAUS KASSNER and C. MISBAH. *Physical Review E*, **66**, 026102 1–9 (2002).
3. I. CANTAT, K. KASNER, C. MISBAH et al. *Physical Review E*, **58,** (5) 6027–40 (1998).
4. K.S. KIM, J.A. HURTADO and H. TAN. *Physical Review Letters*, **83**, (19) 3872–5 (1999).
5. R. ASARO and W. TILLER. *Metall. Trans*., **3**, 1789 (1972).
6. T.J. RENK, P.P. PROVENCIO, T.J. TANAKA et al. *Journal of Nuclear Materials*, **347**, 266–288 (2005).
7. T.J. RENK, C.L. OLSON T.J. TANAKA et al. *Fusion Eng. Des*., **65**, 399 (2003).
8. T.J. RENK, C.L. OLSON T.J. TANAKA et al. *Journal of Nuclear Materials*, **329-333**, 726–731 (2004).
9. J.F. LATKOWSKI R.P. ABBOTT R.C. SCHMITT B.K. BELL *Journal of Nuclear Materials*, **247**, 255-265, (2005).
10. JOHN SETHIAN, R. RAFFRAY, J. LATKOWSKI et al. *Journal of Nuclear Materials*, **347**, 161–177 (2005).
11. W.H. YANG and D.J. SROLOVITZ. *J. Mech. Phys. Solids*. **42**, 1551-1574 (1994).
12. A.A. BECKER. McGraw-Hill International (UK) Limited, (1992).
13. H. GAO. *Int. J. Solids Struct.* **28**, 703-725 (1991).